The sol–gel route: A versatile process for up-scaling the fabrication of gas-tight thin electrolyte layers

Céline Viazzi [a,*], Vincent Rouessac [b], Pascal Lenormand [c], Anne Julbe [b], Florence Ansart [c], Christian Guizard [a]

[a] LSFC, UMR CNRS/Saint-Gobain 3080, CREE, 550 Av. A. Jauffret, BP 20224, 84306 Cavaillon, France
[b] IEM, UMR CNRS/ENSCM/UM2, Université Montpellier 2 (CC47), Place Eugène Bataillon, 34095 Montpellier, Cedex 5, France
[c] CIRIMAT, UMR CNRS-Université Toulouse III, 118 Rte de Narbonne, 31062 Toulouse, Cedex 9, France

ARTICLE INFO

ABSTRACT

Sol–gel routes are often investigated and adapted to prepare, by suitable chemical modifications, sub-micronic powders and derived materials with controlled morphology, which cannot be obtained by conventional solid state chemistry paths. Wet chemistry methods provide attractive alternative routes because mixing of species occurs at the atomic scale. In this paper, ultrafine powders were prepared by a novel synthesis method based on the sol–gel process and were dispersed into suspensions before processing. This paper presents new developments for the preparation of functional materials like yttria-stabilized-zirconia (YSZ, 8% Y_2O_3) used as electrolyte for solid oxide fuel cells. YSZ thick films were coated onto porous Ni-YSZ substrates using a suspension with an optimized formulation deposited by either a dip-coating or a spin-coating process. The suspension composition is based on YSZ particles encapsulated by a zirconium alkoxide which was added with an alkoxide derived colloidal sol. The in situ growth of these colloids increases significantly the layer density after an appropriated heat treatment. The derived films were continuous, homogeneous and around 20 μm thick. The possible up-scaling of this process has been also considered and the suitable processing parameters were defined in order to obtain, at an industrial scale, homogeneous, crack-free, thick and adherent films after heat treatment at 1400 °C.

1. Introduction

Solid oxide fuel cells (SOFCs) are one of the alternative technologies developed for the production of heat and clean energy. This technology is attractive because it has a high efficiency and has the ability to work with diverse fuel sources [1,2]. Reduction of the working temperature of SOFCs from 1000 °C to 700 °C is a key feature since it would considerably increase the life time of the stacks and decrease the system cost [3]. The reducing of the electrolyte thickness, for IT-SOFCs (intermediate temperature SOFCs), is an important challenge since it is a way to decrease the resistance of this key component and, consequently, to reach satisfactory electrochemical performances. Nevertheless, the lower the electrolyte thickness, the higher is the risk for obtaining leaks and defects. A gas-tight electrolyte layer is required to prevent a dramatical power reduction [4]. Moreover, a cost effective technology must allow the production of a significant proportion of gas-tight thin (∼10 μm) electrolyte layers, thus limiting the process yield loss.

Wet chemical routes are cost effective deposition techniques since there is no need for sophisticated systems to coat the substrate [5]. Optimized slurry is typically used to prepare electrolyte layers by dip coating an anodic substrate and withdrawing it at a controlled rate. It is obvious that homogeneous and well dispersed suspensions are required in order to avoid crack formation during the drying and/or firing steps [6,7]. Another strategy is to use the sol–gel route that is a well-adapted process to deposit thin layers (<1 μm), starting from chemical precursors instead of powders as starting materials [8–10]. In this case, the homogeneity of the suspension (sol) is excellent at the molecular level. Moreover, the sol–gel route may generate nanostructured materials with attractive surface properties and reactivity. However, for the fabrication of SOFC electrolytes, multiple deposition steps might be required with classical sols, to reach the target thickness. Intermediate pre-heating and annealing treatment are usually performed. Such a repetitive procedure is time/energy consuming, with high risk for defect formation during the drying steps. This process, in which chemicals are often expensive, is not suitable for up-scaling the production of electrolyte layers. That is the reason why, mixed sol–gel/suspension procedures are considered for preparing, in a single step, thick coatings for either SOFCs [11–13] or, more recently, thermal barrier applications [14,15].

* Corresponding author. Present address: EI CESI, rue Magellan, BP 87501, 31675 Labège, France. Tel.: +33 561003831; fax: +33 561003839.
E-mail addresses: cviazzi@cesi.fr, celine.viazzi@netcourrier.com (C. Viazzi).

In this study, the mixed sol–gel/suspension strategy has been adapted in order to produce gas-tight electrolytes at laboratory scale but with a view towards up-scaling. Two deposition techniques were compared: dip-coating and spin-coating. In addition, the relations between the sol/suspension formulation parameters and the coating gas-tightness have been studied and discussed. Then, gas permeability measurement characterizations were performed in order to characterize the fabricated anodic half cells (porous anode + deposited electrolyte).

2. Experimental

2.1. Materials

A supported anode design was selected, with a planar configuration. The anodes were fabricated by Saint-Gobain according to a process developed by Jülich [16] from a mixture of nickel oxide and yttria-stabilized zirconia (YSZ, 8 mol% Y_2O_3). The roughness of this porous substrate is equal to 1.7 μm (Ra).

The preparation of successful half-cells depends on the optimization of two synthesis steps. First of all, sol formulations have to be adapted to minimize the thermomechanical stresses and secondly, the thermal treatment has to be adjusted to ensure an efficient co-firing without any crack formation but with satisfactory densification (>95%).

Composite sols were formulated by adjusting the proportions of three parts [17]: (a) an organic suspension of YSZ precursor, (b) a YSZ precursor composite sol obtained by introducing the YSZ powder into a YSZ precursor sol synthesized using the alkoxide route [18], and (c) a polymeric matrix synthesized by the Pechini process [19]. Each part of the composite sols was thought to bring a particular contribution towards homogeneous and crack free YSZ layers. The organic suspension (a) is needed to reach sufficient YSZ thicknesses in a single deposition step by increasing the deposited quantity of matter. The composite alkoxide sol (b) promotes a brick-mortar [20] effect during the sintering step of the coating. Indeed, in situ crystallization of YSZ particles from the alkoxide sol improves the coating density [12]. Finally, the polymeric matrix (c) is used as a binder. A detailed description of all the composite sol parts is given below:

(a) YSZ powder (Tosoh, average particles size of 40 nm) containing 8 mol% Y_2O_3 was chosen to formulate 50 wt% loaded suspensions. The solvent was the azeotropic mixture of ethanol–methylethylketone (MEK–EtOH) and 3 wt% (in reference of the total YSZ mass) of an electrosteric dispersant (CP213–CECA) was used in order to disperse the YSZ powder. In addition, sonication (200 W for 30 s using volume of 20 mL) was used to break up the aggregates.

(b) The YSZ colloidal sol was prepared from zirconium *n*-propoxide (Aldrich, 70 wt% in isopropanol), *n*-propanol (Acros Organics, +99%), yttrium nitrate (Acros Organics, 99.9%), acetylacetone (acac, Aldrich) and distilled water. The synthesis parameters were the following: $C = 0.5$ mol L^{-1} for the zirconium, atomic ratio $R' = [acac]/\{[Zr(OC_3H_7)_4] + [Y(NO_3)_3]\} = 0.7$ and $W' = [H_2O]/\{[Zr(OC_3H_7)_4] + [Y(NO_3)_3]\} = 10$ for the hydrolysis ratio. The derived sols were homogeneous, clear and transparent, and consisted of very small colloidal primary particles about 2–3 nm [21]. Then, a part of pre-hydrated YSZ powder (YSZ$_p$, Tosoh) was introduced in this sol. The condensation reactions occur then at the surface of the oxide particles (encapsulating technique) leading to stable suspensions. The ratio Rc gives the weight proportion of pre-hydrated YSZ powder (YSZ$_p$, Tosoh) in the sol: Rc = YSZ$_p$/sol. On the basis of the results reported in [17], this ratio was fixed to 0.11 for all the present study.

(c) The polymeric matrix based on the Pechini method was obtained by polymerization and polycondensation reactions between hexamethylenetetramine (HMTA, Acros Organics, 99%) and acac in acetic acid (VWR) media. The sol viscosity was adjusted by controlling its temperature using a water bath.

The weight proportions between the three components of the composite sols are defined by the following Ra and Rm parameters: Ra = $(b)/(a)$ and Rm = $\{(a)$ and $(b)\}/(c)$. Unless otherwise stated, the samples were fabricated by using YSZ composite sols made from a polymeric matrix with a viscosity of 45 mPa s and the ratios Rm and Ra were, respectively equal to 0.20 and 0.17.

2.2. Rheological characterization of the sols

The flowing behavior of the suspensions was studied at 25 °C with a controlled stress rheometer (MCR301, *Anton Paar GmbH*) using a cylindrical configuration. The shear range lies between 10 and 2000 s^{-1}. This parameter was increased by steps and then decreased. The measurement sequence was repeated twice for each sample to check reproducibility.

2.3. Deposition techniques

Two deposition methods were compared: dip-coating and spin-coating. The dip-coating technique consists in controlling the immersion and withdrawal speeds of a substrate inside a liquid phase. The dip-coating device was manufactured by *Concoat*. The immersion and withdrawal speeds were adjusted in order to control the coating thickness. However, in our case, the Landau and Levich law [22] cannot be used in order to predict the coating thickness because this law is not valid when porous substrates and composite sols are used.

A spin-coater manufactured by *POLOS* was used in order to deposit the electrolyte by the spin-coating technique. This technique consists in depositing a liquid phase on the substrate and to spread this material thanks to a rotational movement. The accelerating speed, the rotational speed and time can be adjusted to obtain homogeneous coatings. Similar to the dip-coating technique, no mathematical law can be used in order to predict the coating thickness for similar reasons.

The heat treatment, in air, was optimized in order to both remove organic compounds and promote a good sintering process. The heating rate was equal to 60 °C h^{-1} up to 410 °C with a dwell time of 4 h, then a heating rate of 120 °C h^{-1} was used up to 1400 °C for 5 h. By using this heat treatment, the amount of shrinkage of the previously described substrate during the co-firing process is about 10%.

2.4. Microstructural characterization of the coatings

The evolution of the coating morphology after annealing was investigated by a scanning electron microscope (SEM) equipped with a solid state backscattering detector (TM1000, *Hitachi*).

2.5. Permeability characterization

The gas-tightness of the sintered coatings was measured at room temperature with a home made set-up. A stainless steel cell, used in dead-end mode and equipped with Vitton® O-rings, has been designed for fitting the half cell (electrolyte/anode). Both sides of the cell were first carefully outgassed in vacuum ($P < 1$ mbar) for 1 h and isolated. The set-up was used first to measure the permeance π_i (mol m^{-2} s^{-1} Pa^{-1}) of He or N_2 as a function of the mean applied pressure up to 5 bar. Contributions of viscous flow and Knudsen diffusion due to macro and nanodefects, if any, can be easily detected
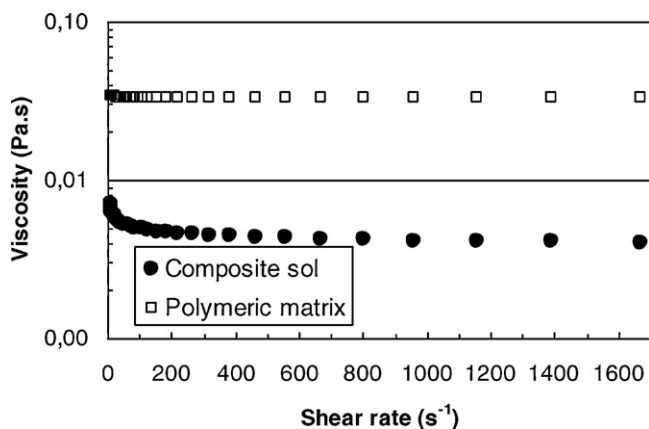
Fig. 1. Evolution of viscosity vs. shear rate for the polymeric matrix and for the derived composite sol.

by this method (screening test). The gas tight samples identified with this simple protocol were further studied with a second protocol in order to better quantify the quality of the coatings. Starting again from the evacuated and isolated cell, a gas i (either He or N_2) was introduced in the electrolyte side at a specific pressure P_i, and the rise of the P_i' pressure on the anode side was measured as a function of time (t). This approach, called time-lag permeation technique, is typical for measuring the permeance π_i and diffusion coefficient D_i of a gas i through dense polymer membranes [23]. By plotting the curve $P_i' = f(t)$, both the time-lag (θ_i) and the slope of the straight line (dP_i'/dt) can be measured for a given pressure of the gas i on the anode side.

According to the second Fick law, the diffusion coefficient D_i is related to the time lag θ_i by the following equation: $D_i\,(m^2\,s) = e^2/(6\theta_i)$, where e is the membrane thickness.

According to the first Fick law, the slope of the linear part dP_i'/dt, is related to the membrane permeance at a given pressure P_i of the gas i, by the following equation: $\pi_i = (dP_i'/dt)(V/(RT\,S\,\Delta P_i))$ where V is the cell volume on the anode side, R is the gas constant, T is the temperature, S is the effective electrolyte surface and ΔP_i is the applied pressure of gas i.

This type of measurement has been used to check the quality of the coating and the reproducibility of the synthesis method.

3. Results and discussion

3.1. Rheological characterization of the composite sol

The rheological behavior of both the polymeric matrix and the derived composite sol has been characterized. As shown in Fig. 1, the viscosity of the polymeric matrix does not depend on the applied shear rate (Newtonian rheological behavior). The viscosity of the composite sol is lower than the polymeric matrix one and it appears to have a slight rheofluidifying behavior for low shear rates values. Indeed the viscosity of the composite sol significantly decreases by increasing the shear rate from 0 to about $150\,s^{-1}$. Then, the sol viscosity remains independent on the shear rate, revealing again a Newtonian behavior. The evidenced rheofluidifying behavior of sols is attractive for coating fabrication. Indeed, such a behavior favours the spreading of slurries on the substrate when a movement is operated during the deposition. On the other hand, the Newtonian behavior guarantees that the slurry remains homogeneous and well dispersed, which is of prime importance to obtain uniform coatings. In the present study, a sol with a Newtonian behavior is also attractive for comparing different deposition techniques without needing to modify the sol formulation.
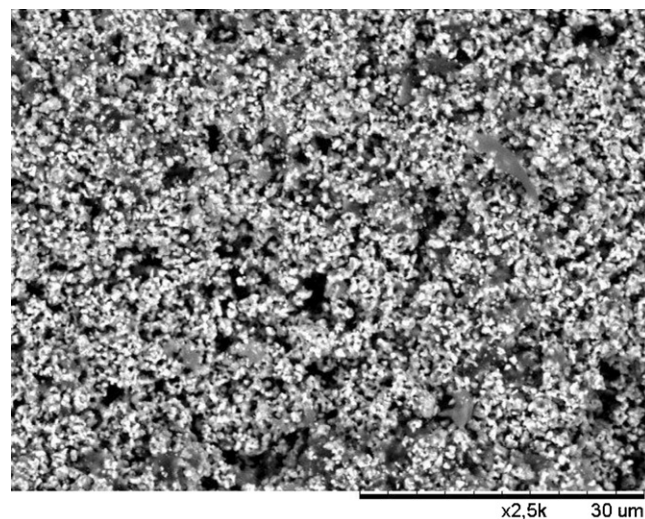

SG-CREE

Fig. 2. SEM observation of the surface of the porous anode.

3.2. YSZ layers obtained by the dip-coating technique

The dip-coating technique is well adapted to the deposition of homogeneous layers (<200 μm) on substrates with complex shapes and is also very attractive for scaling-up on large substrate sizes. It is thus a possible technical option for planar SOFC configurations. That is the reason why the potential of this technique was evaluated for single step deposition of YSZ layers on anode substrates. Fig. 2 shows the surface of the virgin anode substrate. The backscattered electron detector identified both YSZ and NiO compounds uniformly distributed in the porous support.

A first YSZ layer was deposited on this anode substrate by employing immersion and withdrawal rates of $1\,cm\,s^{-1}$ and $0.3\,cm\,s^{-1}$, respectively. Then, a thermal treatment was performed in order to slowly remove the organics and to promote the sintering of the electrolyte layer at 1400 °C. A typical supported layer obtained in these conditions is shown in Fig. 3. The YSZ coating is very homogeneous and no infiltration of the composite sol in the anode porosity is observed. However, a residual porosity can be detected in the densified coating that is certainly due to the
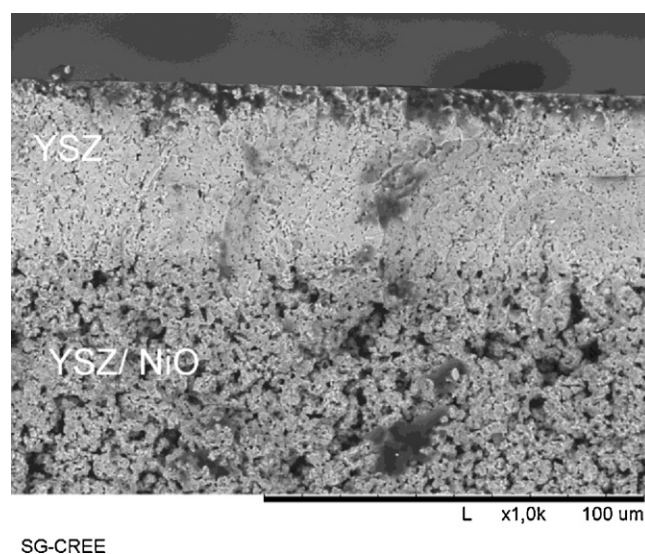

SG-CREE

Fig. 3. Cross-section of a typical sample obtained using the dip-coating technique and a composite sol.
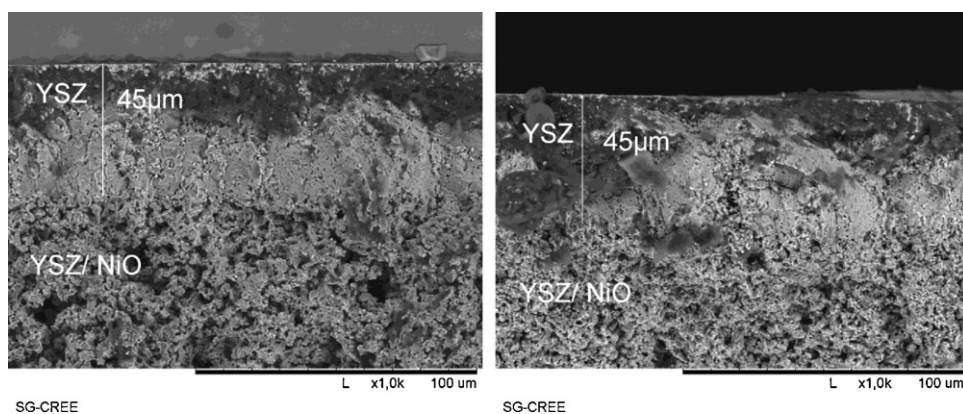
Fig. 4. Cross-sections of YSZ coatings deposited on the anode material by using the dip-coating technique with an immersion rate of $1.0\,cm\,s^{-1}$ and a withdrawal rate of either $0.7\,cm\,s^{-1}$ (left) or $1.3\,cm\,s^{-1}$ (right). The black material at the top of the YSZ layer is due to the cutting of the sample.

removal of the organic parts and to the co-firing treatment. The coating thickness is 45 μm and is higher than the target thickness for IT-SOFC applications.

Two other withdrawal rates, $0.7\,cm\,s^{-1}$ and $1.3\,cm\,s^{-1}$, were tested in order to try to decrease the electrolyte thickness, while keeping constant the immersion rate at $1\,cm\,s^{-1}$. The cross-sections of the derived samples obtained after the firing step are shown in Fig. 4. Whatever the withdrawal rate, the coating microstructure was unchanged and, the coating thickness was poorly modified.

YSZ coatings were also manufactured by increasing the immersion rate of the anode up to $2.0\,cm\,s^{-1}$ (withdrawal rate: $1.3\,cm\,s^{-1}$). The cross-section of the corresponding sample, after the firing step, is shown in Fig. 5. Again, the microstructure of the YSZ layer is unchanged, but a twice thinner YSZ layer is obtained: the thickness is 25 μm for an immersion rate of $2.0\,cm\,s^{-1}$ instead of 45 μm for an immersion rate of $1.0\,cm\,s^{-1}$. The support immersion rate is consequently a key parameter for controlling the thickness of the deposited coating This result brings out the importance of the hydrodynamic parameters during the deposition process, which are related both to the substrate surface quality (roughness and porosity) and to the composite sol formulation (viscosity, ceramic loading) [24]. In our experiments, increasing the immersion rate of the anode in the composite sol strongly modifies the process hydrodynamics and consequently the coating thickness.
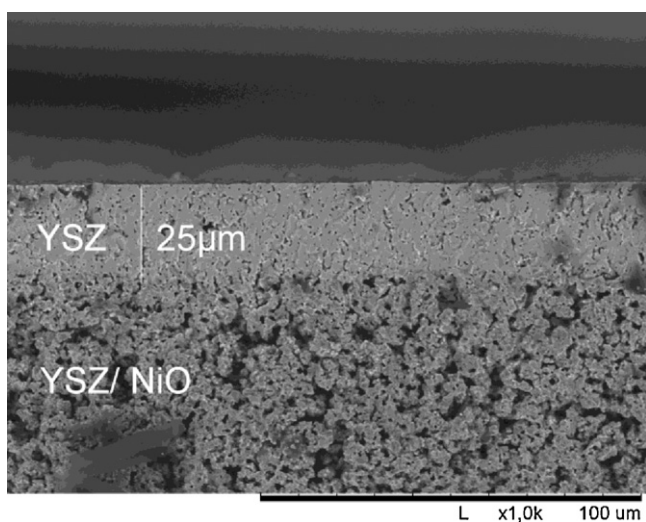

Fig. 5. Cross-section of a YSZ coating deposited on the anode by using the dip-coating technique with an immersion rate of $2.0\,cm\,s^{-1}$ and a withdrawal rate of $1.3\,cm\,s^{-1}$.

3.3. Transfer to the spin-coating technique

For planar SOFC configurations with two-chambers, the electrolyte has to be deposited only on one side of the cermet anode. Then, when using the dip-coating technique to deposit this functional layer, one face of the cermet support has to be masked. This time-consuming step may be critical since the anode is porous and consequently hard to mask efficiently. As a result, this additional procedure often implies uncontrolled slurry infiltration above the mask and also edge effects caused by inhomogeneous coating thickness near the mask. This latter effect can generate cracks in the coating during the drying or firing steps, which are detrimental to SOFC applications. Consequently for planar configurations, the spin-coating technique appears to be more suitable because only one anode face can be coated without any mask being required.

Coatings were deposited on the anode by spin-coating, in a single step, by using an acceleration rate of $1000\,rpm\,s^{-1}$ and a rotational rate of 6000 rpm for 15 s. From a macroscopic point of view, these conditions were ideal for homogeneously coating the whole sample surface ($\sim4\,cm^2$). The cross-section of the derived sample is shown in Fig. 6. After the firing step, the morphology/microstructure of the spin-coated layers are absolutely similar to that of dip-coated ones. Indeed, no infiltration of the sol inside the substrate porosity is noticed and the electrolyte/anode interface is clearly defined. The thickness of the YSZ layer deposited in a single step (10 μm) typically fits the requirements for IT-SOFC application.

3.4. Up-scaled deposition process using the spin-coating technique

In order to evaluate the potential of the above strategy for scaling-up the fabrication of thin supported electrolyte layers, four times larger anodes ($16\,cm^2$ instead of $4\,cm^2$) were considered. The objective was to clearly identify the parameters that could have major impacts for larger scaling-up. Two kinds of parameters were found to influence the coating homogeneity: the parameters relative to the composite sol formulation and those corresponding to the spin-coating conditions.

A composite sol with the previously optimized formulation ($Ra = 0.16$, $Rm = 0.2$, with a polymeric matrix of 45 mPa s) was used for coating the anode support by spin-coating ($1000\,rpm\,s^{-1}$, 6000 rpm, 15 s). By keeping constant these parameters, macroscopic radial striations of the sample surface were observed. Besides, no improvement of the coating quality was obtained by increasing the rotational rate up to 3000 rpm (radial striations still observed). This result highlights the inhomogeneity of YSZ layers
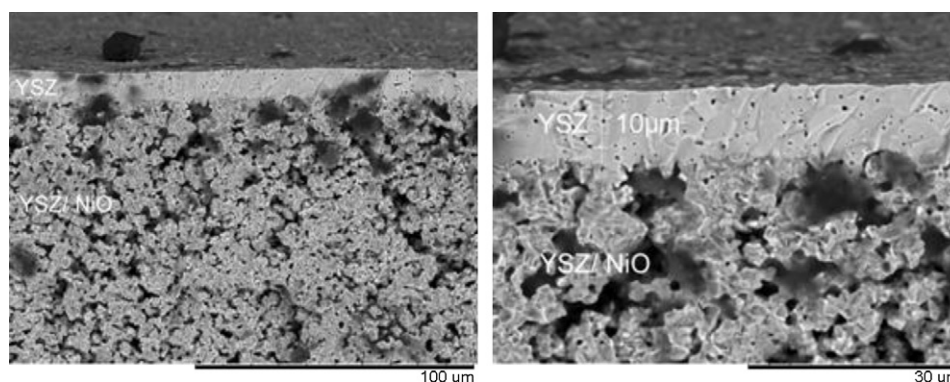
Fig. 6. Cross-section of an YSZ coating deposited on the anode by using the spin-coating technique with an accelerating rate of 1000 rpm s^{-1} and a rotational rate of 6000 rpm for 15 s.

Table 1
Microstructural observations and qualitative tightness evaluation of the YSZ layers deposited by spin-coating on porous anodes, and co-fired at 1400 °C for 5 h.

	Rotational rate (6000 rpm)			Rotational rate (3000 rpm)	
	A	B	C	D	E
Rm	0.17	0.20	0.25	0.20	0.25
Radial striations	Yes	Yes	**No**	Yes	**No**
Infiltration of water drops	Yes	Yes	Yes	Yes	**No**

The bold indications highlight the more appropriate properties.

on large anodes. In order to evaluate the coating quality in terms of defects (cracks, uncompleted sintering, residual connected pores, etc.), the simple and rapid water drop test [25] has been first performed on the anode supported YSZ layer after co-firing at 1400 °C. The test just consists in observing the behavior vs. time of water droplets. If water is rapidly (<5 min) drained through the YSZ layer by capillary effects, the presence of defects in the coating is obvious. In the case of the two lastly mentioned samples with radial striation, the water drops deposited at the outer ring of the anode and without contact with the edge, were drained after 1 min. On the other hand, the droplets deposited in the sample center stayed for more than 5 min, thus proving that coating quality was not uniform and that defects were present in the outer ring of the coating. These defects can easily be associated with a lower thickness far from the anode center. Indeed, the thinner is the coating, the more difficult it is to obtain continuous and crack-free layers on the rough porous anode. In the present case, a modification of the rotational rate was not the adequate strategy to improve the coating quality.

Consequently, in order to adapt the process to larger sample size, we decided to modify the composite sol formulation. We only adjusted the polymeric matrix composition since the major role of this polymer is to act as a dispersing matrix for the YSZ particles in the composite sols as it was checked in Section 3.1 dedicated to rheological characterization. Also it was necessary to find a good compromise between the proportion of organics required for efficient sol dispersion, and the maximum quantity for which irreducible cracks will begin to form during the debinding step. That is the reason why, the initial viscosity of the polymeric matrix was identified as the key factor to improve the coating quality. This approach allows to modify significantly the sol behavior without adding too important proportion of organics.

New composite sols were then formulated using a polymeric matrix with a lower viscosity than previously, in order to spread more easily the composite sol on the anode surface. A sol viscosity of 30 mPa s, instead of 45 mPa s, was obtained by modifying the heating time during the polymer synthesis. Then, the ratio Rm was slightly modified to formulate three composite sols (Table 1). The samples #A, B and C were obtained with a Rm ratio equal to 0.17, 0.20 and 0.25, respectively (rotational rate: 6000 rpm).

Several radial striations were still visually observed on the surface of samples #A and B that were prepared with the lowest amount of polymeric matrix, although the coating #C corresponding to Rm = 0.25 looked (macroscopically) perfectly uniform. However, the water drops deposited on the more external part of the YSZ layer were drained in less than 1 min, showing that the microstructure and thickness of the YSZ coating were not homogeneous on the whole anode surface.

In order to further increase the coating thickness homogeneity, samples #D and E were prepared using a rotation rate of 3000 rpm. Macroscopically homogeneous coatings were obtained when composite sol with Rm = 0.25 were used and absolutely no infiltration of the water drops was observed for the derived samples (Fig. 7). It is also interesting to note that a slight decrease of the Rm ratio to 0.20 does not generate homogeneous coatings (Table 1, sample #D) and there is no advantage adding more polymeric matrix in

Fig. 7. Water drops deposited on sample E after a co-firing treatment at 1400 °C. The YSZ coating was deposited by the spin-coating technique, using a rotational rate of 3000 rpm and a ratio Rm equal to 0.25 (sample #E). The water drops were not drained after 5 min.
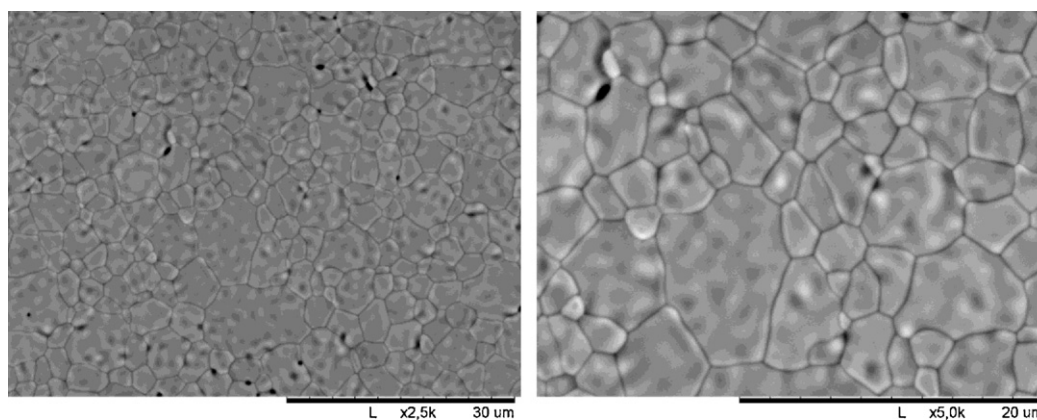
Fig. 8. SEM observations of the surface of the YSZ layer deposited by spin-coating (1000 rpm s^{-1}, 3000 rpm, 15 s) on an anode of 16 cm^2, after a co-firing treatment at 1400 °C (sample #E).

the formulation since it makes more difficult the debinding and sintering stages.

The surface of sample #E is shown in Fig. 8. No defect is observed in the layer except, a small number of residual pores, that is in major part due to the removal of the organics. Fig. 9 shows a cross-section of the corresponding anodic half-cell which is about 14 µm thick. The microstructure of the densified YSZ layer is similar to those previously obtained. Indeed, there is no infiltration of the composite sol inside the anode porosity and the interface between the densified YSZ coating and the porous substrate is well defined.

In conclusion, the polymeric matrix appears to have the most significant effect on the homogeneity of the spin-coated layers. It has to be adjusted together with the spin-coating parameters in order to optimize the homogeneity of the YSZ layers. We demonstrated that it is possible to fabricate, in a single step, a 10 µm thick YSZ uniform layer on a relatively large porous anode (16 cm^2) by using the spin-coating technique and an optimized composite sol formulation. In order to further evaluate the quality (tightness) of the YSZ coatings, gas permeability measurements have been performed on sample D.

3.5. Permeability characterization

Due to the sealing (O-ring) of the permeation test cell, the sample (the anode disc support coated with the electrolyte) should be
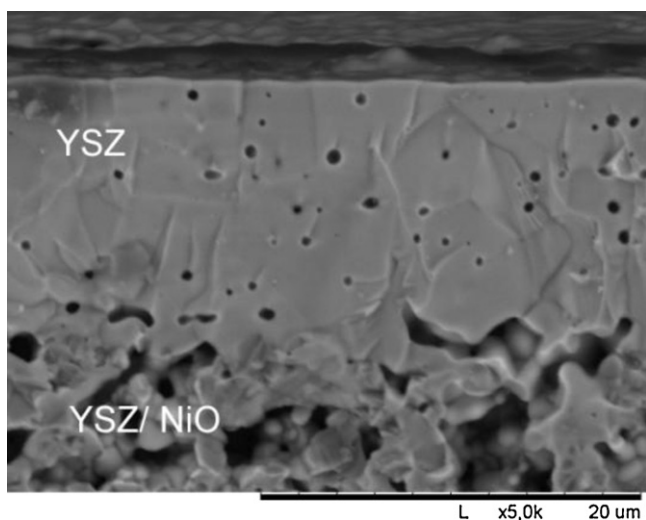

Fig. 9. SEM observation of the cross-section of a YSZ layer deposited by spin-coating (1000 rpm s^{-1}, 3000 rpm, 15 s) on an anode of 16 cm^2, after a co-firing treatment at 1400 °C (sample #E).
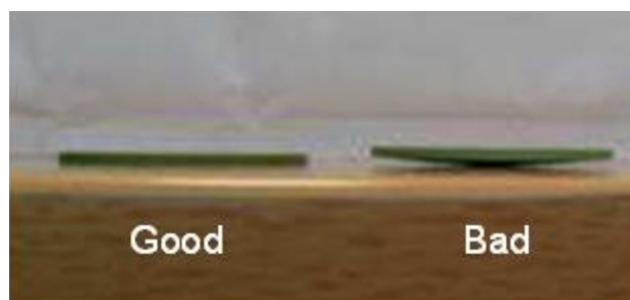

Fig. 10. Optical photographs of two anode discs after the 1400 °C sintering. The right one is not flat enough in order to characterize the gas-tightness of the top electrolyte in the lab-scale permeation cell.

flat after sintering otherwise it breaks, even after a low tightness rating.

Once this technical lock has been fixed (Fig. 10), permeation and gas-tight measurements can be carried out with success. This can be achieved thanks to an ironing step at 1350 °C during 1 h. This additional treatment was performed, separately, after the sintering step by using loads in alumina. All permeation results have been corrected from the weak natural leak of the set-up.

Whereas preliminary samples followed a viscous flow behavior as the gas permeance (π_i) linearly increased when the transmembrane pressure (ΔP_i) increased, helium and nitrogen tight samples (anode covered with electrolyte) have been obtained applying to the first protocol (described in Section 2.5) up to the transmembrane pressure $\Delta P_i = 4$ bar.

In order to better characterize the gas tightness efficiency of the electrolyte, the second protocol has then been applied in a dead-end mode. Fig. 11 presents the pressure (P') evolution on the anode side following a sudden feed of $P = 5$ bar of pure He on the electrolyte side. From this type of evolution, diffusion coefficients and permeance of pure nitrogen or helium have been extracted. Table 2 lists one flat anode covered by a 20 µm-thick electrolyte. These important diffusion coefficients are due to the defects and do not represent the gas permeabilities through the bulk material. In best cases, D_{He} and D_{N_2} were few 10^{-14} m^2 s^{-1} and π_{He} and π_{N_2} were few 10^{-10} mol m^{-2} s^{-1} Pa^{-1}. Such figures are in an acceptable range

Table 2
Gas permeation characteristics of the surface barrier electrolyte.

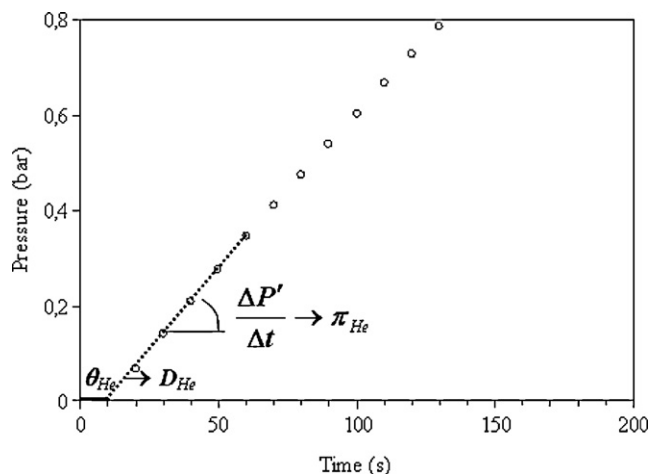| i	Diffusion coefficient D_i (10^{-12} m^2 s^{-1})	Permeance π_i (10^{-9} mol m^{-2} s^{-1} Pa^{-1})
Nitrogen	2.95	7.4
Helium	8.98	10.7

Fig. 11. Progressive increase of the helium pressure at the anode side, following a sudden introduction of 5 bar of helium at the electrolyte feed side.

and consistent with such dense materials and show that the scale up process by spin-coating is successful.

4. Conclusions

An alternative experimental process combining either dip-coating or spin-coating method with optimized slurry formulations was developed to prepare YSZ thin films on porous Ni–YSZ substrates. The slurries (or composite sols) consist of a YSZ commercial powder suspension in organic media (dispersing solvent), mixed to a sol derived from zirconium alkoxide and yttrium salt in a polymer matrix. The derived layers are continuous, homogeneous and adherent, and their microstructure is significantly dense without any connected open porosity as it was proved by the permeability measurements. The optimized film thickness is in the range 10–20 μm, which fits the requirements for SOFC electrolytes working at 700 °C (IT-SOFCs).

As a conclusion, an original low cost and versatile process has been developed in this work which is well adapted to the preparation of dense YSZ layers on porous anodes of at least 16 cm^2 by adjusting experimental formulation parameters. Both a single deposition step and a single thermal treatment are needed to obtain the required film quality. This is particularly attractive for an industrial development of the protocol. In parallel to these up-scaling studies, further work is now in progress for trying to replace the organic media by an aqueous media. This is motivated both by

environmental and economical requirements. Indeed the use of volatile organic compounds is now severely controlled on industrial sites. Furthermore alkoxide precursors are highly reactive with water and are much more expensive than metallic salts. The latter, if adapted to the protocol, should then be much more favourable for the development of a cost-effective and green process.

References

[1] B.C.H. Steele, A. Heinzel, Nature 414 (6861) (2001) 345–352.
[2] N.Q. Minh, Solid State Ionics 174 (1–4) (2004) 271–277.
[3] B.C.H. Steele, Solid State Ionics 134 (1–2) (2000) 3–20.
[4] T. Van Gestel, D. Sebold, W.A. Meulenberg, H.-P. Buchkremer, Solid State Ionics 179 (11–12) (2008) 428–437.
[5] D. Beckel, A. Bieberle-Hütler, A. Harvey, A. Infortuna, U.P. Muecke, M. Prestat, J.L.M. Rupp, L.J. Gauckler, Journal of Power Sources 173 (2007) 325–345.
[6] Y. Zhang, J. Gao, D. Peng, M. Guangyo, X. Liu, Ceramics International 30 (2004) 1049–1053.
[7] Y.H. Wang, X.Q. Liu, G.Y. Meng, Ceramics International 33 (6) (2007) 1025–1031.
[8] A. Julbe, C. Guizard, A. Larbot, L. Cot, A. Giroir-Fendler, Journal of Membrane Science 77 (1993) 137.
[9] R. Vacassy, C. Guizard, V. Thoraval, L. Cot, Journal of Membrane Science 132 (1997) 109.
[10] L. Cot, A. Ayral, J. Durand, C. Guizard, N. Hovnanian, A. Julbe, A. Larbot, Solid State Science 2 (2000) 313.
[11] P. Lenormand, D. Caravaca, C. Laberty-Robert, F. Ansart, Journal of the European Ceramic Society 25 (2005) 2643–2646.
[12] F. Ansart, J.-P. Bonino, P. Lenormand, Ch. Laberty-Robert, C. Viazzi, Key Engineering Material 317–318 (2006) 529–532.
[13] P. Lenormand, M. Rieu, R.F. Cienfuegos, A. Julbe, S. Castillo, F. Ansart, Surface and Coatings Technology 203 (2008) 901–904.
[14] C. Viazzi, J.P. Bonino, F. Ansart, Surface and Coatings Technology 201 (2006) 3889–3893.
[15] J. Fenech, C. Viazzi, F. Ansart, J.-P. Bonino, Advanced Materials Research 89–91 (2010) 184–189.
[16] Fuel Cells Bulletin 12 (2006) 3.
[17] F. Mauvy, P. Lenormand, C. Lalanne, F. Ansart, J.M. Bassat, J.C. Grenier, Journal of Power Sources 171 (2) (2007) 783–788.
[18] D.C. Bradley, D.G. Carter, Canadian Journal of Chemistry 39 (1961) 1434–1443.
[19] P. Pechini, US Patent 3,330,697 (July 11, 1967).
[20] X. Wang, W.H. Lan, P. Xiao, Thin Solid Films 494 (1–2) (2006) 263–267.
[21] A. Lecomte, A. Dauger, P. Lenormand, Journal of Applied Crystallography 33 (2000) 496–499.
[22] L.D. Landau, V.G. Levich, Acta Physica Chimica USSR 17 (1990) 42.
[23] S.W. Rutherford, D.D. Do, Adsorption 3 (1997) 283–312.
[24] H. Benkreira, Chemical Engineering Science 59 (2004) 2745–2751.
[25] E.W. Washburn, Physical Review 17 (3) (1921) 273–283.